J. Fluid Mech. (1985), *vol.* 150, *pp.* 139–158
Printed in Great Britain

The upstream scale of flow development in curved circular pipes

By D. E. OLSON AND B. SNYDER

Pulmonary Disease Unit, Veterans Administration Medical Center/University of Michigan, Ann Arbor, Michigan 48105

(Received 26 September 1983 and in revised form 17 January 1984)

For steady airflows at moderate Dean number ($100 \leqslant \kappa \leqslant 500$) axial- and transverse-velocity profiles were delineated by anemometry in the entry region of curved circular pipes, having curvature ratios R/a of 4.66 or 8. Uniform inlet velocity profiles were found to evolve downstream over two inviscid length scales. Axial profiles develop on the lengthscale a, the pipe radius. The upstream influence extends at least $6a$ into a bend. Within this region axial development is largely inviscid and apparently independent of the radius of curvature R. Secondary currents develop on the scale $(aR)^{\frac{1}{2}}$. Their initial growth is consistent with a model of vorticity transport based on streamline curvature, but instead of progressing monotonically to an asymptotic value, this swirl first overshoots, then subsides approximately $2(aR)^{\frac{1}{2}}$ downstream from the inlet. Hawthorne's model of streamline twist appears to account qualitatively for this dampening.

1. Introduction

It is well known that steady flows through tightly-curved circular pipes generate large-scale swirling motions involving the entire flow stream, as seen in the flow pattern of figure 8. In one numerical study, peak secondary currents within the boundary layer were computed by Yao & Berger (1975) to be greater than mainstream axial velocities, even at a moderate Dean number of 894. As such currents produce rapid mixing, a quantitative understanding of their development would have wide application to engineering and physiological flow systems. Much insight is contained in the study of Agrawal, Talbot & Gong (1978), who used laser-Doppler anemometry (of glycerol–water solutions) to illustrate how downstream axial and transverse velocity profiles evolve from laminar flat inlet flow. The present investigation, which stems from Olson's (1971) study of laminar airflow in the first 180° of bend in tightly curved pipes, is intended to resolve what lengthscales describe flow development over entrance lengths typical of practical flow devices.

In interpreting our results we have often referred to Yao & Berger's theoretical study of flow development in curved pipes. By matching mainstream flow to boundary-layer currents, these authors proposed that secondary flows evolve over two distinct lengthscales. The extents of these two regions are compared in table 1 for our experimental curvature ratios R/a = radius of pipe curvature/pipe radius, Reynolds numbers $Re = 2\overline{W}a/\nu$ and Dean numbers $\kappa = (a/R)^{\frac{1}{2}} Re$. In an upstream region extending over a path length $L \sim 0.1(aR\kappa)^{\frac{1}{2}}$ the development of secondary flow is expected to be largely inviscid, being scaled to the axial length parameter $(aR)^{\frac{1}{2}}$. The last apparent vestiges of this inviscid regime disappear by 0.3–$0.5\,(aR\kappa)^{\frac{1}{2}}$, whereupon flow patterns develop asymptotically on a downstream scale $(aR\kappa)^{\frac{1}{2}}$. It

Curvature ratio R/a	Reynolds number Re	Dean number κ	Equivalent straight pipe $L/D \approx 0.06\,Re$	Curved pipe upstream length† $L/D \approx 0.2\,(aR\kappa)^{\frac{1}{2}}/a$	Curved pipe fully developed‡ $L/D \simeq e_1\,(aR\kappa)^{\frac{1}{2}}/2a$
			(*a*) $\overline{W} = 12$ cm/s		
4.66	300	140	18.0	5.1	40.9
8.0	290	103	17.4	5.7	38.8
			(*b*) $\overline{W} = 44$ cm/s		
4.66	1080	500	64.8	9.7	77.2
8.0	1100	390	66.0	11.2	75.4

† Figure 3(*a*, *b*) of Yao & Berger (1975).
‡ Equation 30 of Yao & Berger, with $2.7 \leqslant e_1 \leqslant 3.2$.

TABLE 1. Predicted entry lengths for experimental inlet conditions, expressed in pipe diameters D

is apparent in table 1 that our 180° pipe bends, which extend a length of 7.3 (or 12.6) diameters for $R/a = 4.66$ (or 8), barely enter Yao & Berger's downstream regime. Therefore only their upstream scale $(aR)^{\frac{1}{2}}$ is pertinent to this investigation.

It would be surprising if all the detailed flow structures stemming from a flat inlet profile should evolve over the single lengthscale $(aR)^{\frac{1}{2}}$, since initially swirl is confined to the viscous boundary layer while axial development occurs largely in the inviscid core. Moreover, Yao & Berger used a modal analysis which employed fully developed axial velocity profiles, favouring the outer wall of the pipe bend: by contrast, Singh (1974) showed analytically that a uniform injection velocity forms a potential line vortex that causes flow first to shift inwards, rather than outwards. This inviscid structure, which has been observed experimentally by Agrawal *et al.*, persists downstream in modified form as the core flow accelerates due to boundary-layer displacement, as seen in figure 3(*a*). Its presence could be expected to influence the scale over which upstream structures evolve, and we shall show that two inviscid scales, $(aR)^{\frac{1}{2}}$ and a, are needed to describe flow development in the entrance region.

How axial profiles develop is especially pertinent to the formation of swirl. Hawthorne (1951) proposed that secondary currents in bent pipes are self-limiting: their growth and subsequent dampening are determined in part by the rate at which their streamlines are deflected and twisted by the secondary motion. Since the rate of twist must also depend on how rapidly fluid is convected downstream, the two most prominent flow structures – axial-velocity profiles and transverse currents – must interact to produce downstream flow patterns representative of a particular inlet condition. This report contains quantitative results of this interaction for the special case of a flat inlet profile.

2. Methods

Two circular curved pipes were machined in half sections from Plexiglas, using a semicircular cutter to ensure 1 % geometric accuracy. Internal walls were polished prior to assembling the flow sections, which were 3.81 cm (1.5 in.) inner diameter, extended through 300° of arc, and had curvature ratios R/a of 4.66 or 8. An axial fan supplied steady low-pressure airflow, which was stabilized by passage through an upstream plenum and heat exchanger, then screened and straightened prior to entry into the test section. Volume flow rates were monitored by rotameters to within ± 5 % accuracy.

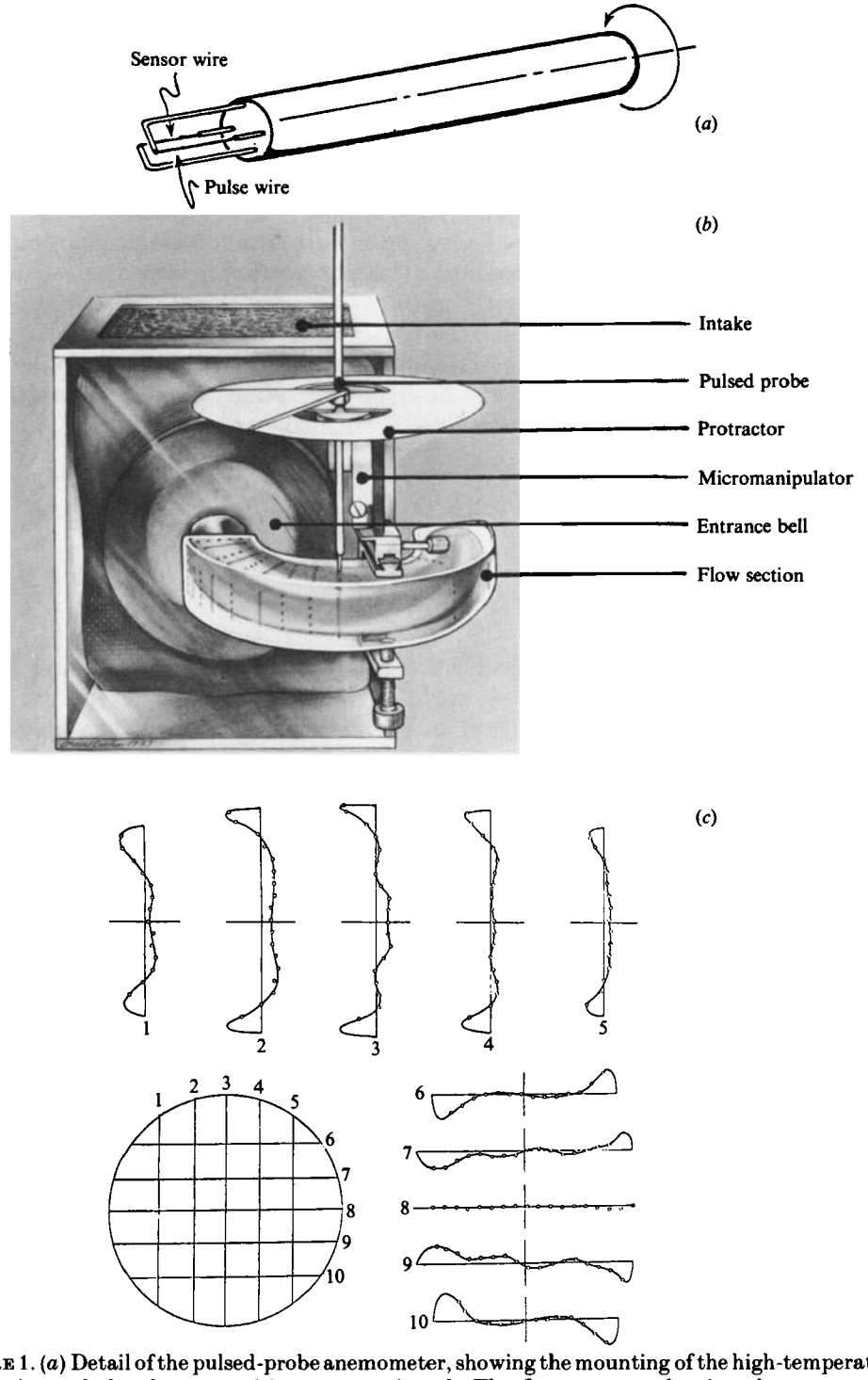

FIGURE 1. (*a*) Detail of the pulsed-probe anemometer, showing the mounting of the high-temperature pulse wire and the thermosensitive sensor wire. (*b*) The flow system, showing the test section mounted on an upstream plenum and entrance bell, and the pulsed-probe anemometer positioned on the pipe wall. (*c*) Configuration of vertical (1–5) and horizontal (6–10) probe traverses, with corresponding X- and Y-components of secondary velocity. Inner wall of pipe bend is towards left. Parabolic inlet velocity profile, $R/a = 4.66$, $\kappa = 510$, $\overline{W} = 45$ cm/s, at 180° of bend. Length and velocity scales: each interval between traverses $= 0.3a = 0.3\overline{W}$ cm/s. (*a*) and (*c*) are from Olson *et al.* (1984); reproduced by permission of ASME.

Transverse (X, Y) and axial (Z) velocity components were measured at selected downstream intervals, using a pulsed-probe anemometer inserted into the flow stream through tightly fitted slots milled into the pipe walls (figure 1*b*). This device, as described by Olson, Parker & Snyder (1984), determines pointwise velocities by measuring the transport time and direction of a thermal pulse initiated at an upstream wire and sensed at a downstream wire thermistor (figure 1*a*). The transport time gives a reproducible measure of local velocity for a given wire separation, determined microscopically. The probe tip was positioned by a micromanipulator at intervals of $0.1a$ along the five vertical and five horizontal traverses shown in figure 1(*c*). Along each traverse the magnitude V_α and direction α of pointwise velocities were found by rotating the probe tip until the velocity signal was maximal. Thus two mutually perpendicular local measurements of speed and direction, (V_α, α) and (V_β, β), were obtained at each intersection point in the cross-sectional grid. Using the empirically determined probe yaw response, all three pointwise velocity components were then computed from the expressions

$$V = V_\alpha(\cos\beta)^{-\frac{2}{3}} = V_\beta(\cos\alpha)^{-\frac{2}{3}} \quad \text{(empirical yaw response)}, \tag{1a}$$

$$V_x = V\sin\alpha\cos\beta(1-\sin^2\alpha\sin^2\beta)^{-\frac{1}{2}}, \tag{1b}$$

$$V_y = V\cos\alpha\sin\beta(1-\sin^2\alpha\sin^2\beta)^{-\frac{1}{2}}, \tag{1c}$$

$$V_z = V\cos\alpha\cos\beta(1-\sin^2\alpha\sin^2\beta)^{-\frac{1}{2}}. \tag{1d}$$

Between intersection points, velocity components were evaluated using linearly interpolated estimates of the yaw angle. Axial-velocity distributions were then integrated over each cross-section to determine volume flow rate, which yielded $\pm 5\,\%$ agreement with the corresponding rotameter reading.

Preliminary testing demonstrated probe position to be resolved to within ± 0.5 mm and direction to within $\pm 1°$. Pointwise velocities usually were repeatible to within $5\,\%$ when the probe was inserted from opposite walls of the pipe, and symmetric to the same degree about the symmetry plane. Therefore we infer that secondary velocities were usually determined to within $\pm 5\,\%$ accuracy.

Table 1 lists the Reynolds and Dean numbers at which the experiments were carried out. Axial and transverse velocity distributions were determined at 20°, 40°, 60°, 90° and 180° of bend angle for flat inlet profiles. These cases were supplemented by examples of downstream distributions derived from parabolic inlet profiles.

Inlet parabolic profiles were formed by connecting a thermally isolated straight pipe 100 diameters in length directly to the inlet of the curved pipes. The velocity profiles labelled 'entrance' in figure 3(*b*) were determined to be within $\pm 1\,\%$ of a parabolic distribution, and the flow direction to be aligned within $\pm 1°$ to the pipe axis. Flat inlet profiles were produced by attaching an entrance bell of empirical design 1.6 cm upstream of the curved pipes. The profiles labelled 'entrance' in figure 3(*a*) were measured at the bell mouth, using a straight outrun of 30 cm attached downstream of the bell to prevent exit effects. Velocity profiles produced by this bell were determined to be flat within $\pm 1\,\%$ in the central region ($0 \leqslant r/a \leqslant 0.75$) of the flow stream and aligned within 1° to the pipe axis. However, we view these results with caution for the following reasons.

Once the straight outruns were replaced by the curved pipes, anemometer measurements taken 3 mm downstream from the onset of pipe curvature (labelled 0° in figure 3*a*) revealed the presence of definite velocity gradients $\partial W/\partial X$ across the horizontal centreline. Thus the inlet profiles were probably distorted by the abrupt

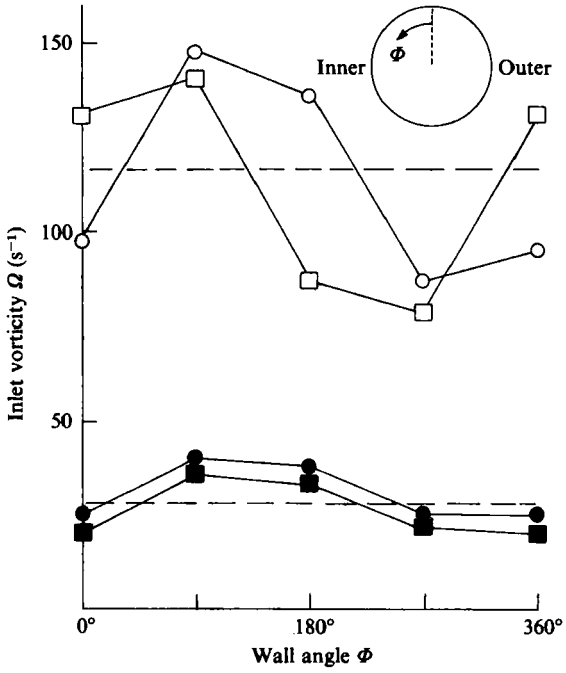

FIGURE 2. The angular distribution of inlet azimuthal vorticity $\Omega = \partial W/\partial r$ in the wall vortex ring, as estimated from wall gradients averaged over $0.8 \leqslant r/a \leqslant 1.0$. Solid lines are hot-wire anemometer measurements taken 3 mm downstream of the inlet; dashed lines are corresponding measurements with the curved pipe replaced by a straight outrun. Inner wall of pipe bend at 90°. Closed symbols, $Re = 300$; open symbols, $Re = 1100$; circles, $R/a = 4.66$; squares, $R/a = 8.0$.

formation of the potential line vortex. It is likely that downstream pressure distributions within our test sections retarded outer-wall velocities upstream of the curved-pipe entrance, as Humphrey, Taylor & Whitelaw (1977) noted for turbulent entrance flows through curved pipes of rectangular cross-section. As it was important to establish how much the resulting inlet profiles deviated from an axisymmetric distribution, the angular distribution of inlet azimuthal vorticity $\Omega = \partial W/\partial r$, averaged over the thickness of the wall vortex ring $0.8 \leqslant r/a \leqslant 1$, was compared in figure 2 with the unperturbed case resulting from a straight outflow. Although the presence of the line vortex results in a much more asymmetric distribution of wall vorticity, mean values fall within 10% of those obtained with an initially flat profile. Moreover, no secondary currents could be detected 3 mm downstream from the inlet.

Consistent with the formation of a line vortex, Agrawal *et al.* have noted that the quantity $G^{-1} = -(W/a)_0 (\partial W/\partial X)_0^{-1}$, evaluated across the horizontal centreline, should equal R/a, the curvature ratio. In our experiments pulsed-probe measurements of axial velocity profiles at 20° of bend yielded values of 5.4 ± 0.5 and 11.0 ± 1.5 for curvature ratios of 4.66 and 8 respectively. This result corresponds to a deviation of less than 3% from an idealized axial profile. We conclude that, while skewed inlet profiles may have altered the earliest stages of flow development, flow patterns $0.75\,(aR)^{\frac{1}{2}}$ or more downstream of the inlet are unlikely to be more than 5% different from those evolving from ideally uniform inlet profiles.

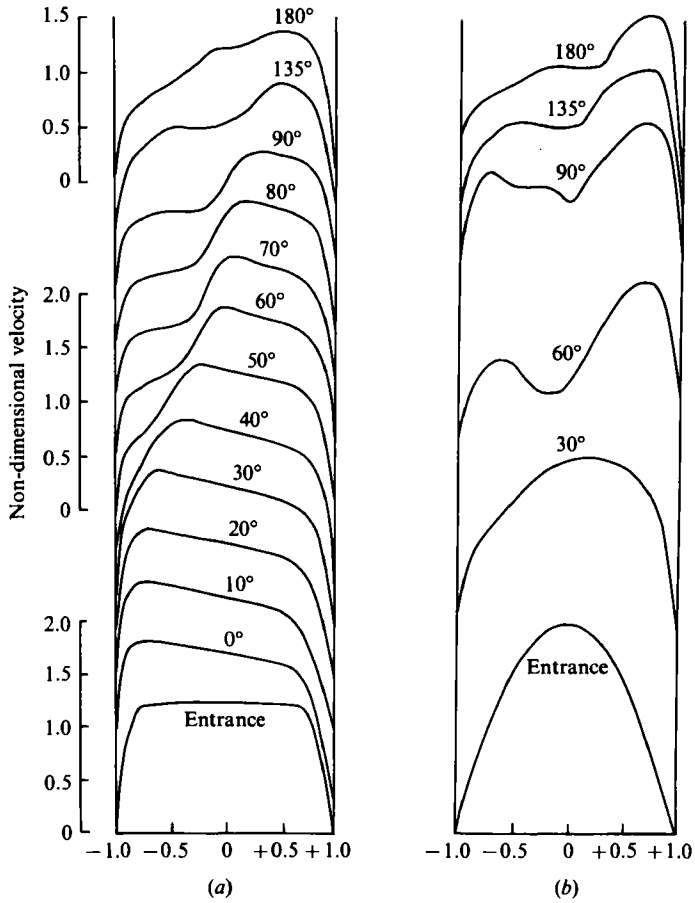

FIGURE 3. Velocity profiles, from hot-wire anemometry, in the symmetry plane at the indicated bend angles: (*a*) flat; (*b*) parabolic inlet profiles. Horizontal axis is non-dimensional pipe radius, with −1.0 at inner wall of bend. Profiles labelled 'entrance' were measured with curved pipe absent; position 0° was 3 mm downstream from the onset of bend. Mean axial velocity $W = 42$ cm/s, $R/a = 4.66$.

3. Results

Preliminary observations of flow development were made by positioning a hot-wire anemometer in the symmetry plane of the bend at several locations downstream from the pipe entrance. Examples of such traces, in figures 3(*a*, *b*), are taken from Olson's complete set of illustrations comprising *Re* between 180 and 1630. It is evident in this figure that flat and parabolic inlet profiles evolve into distinctly different downstream sequences, proving that the influence of the inlet condition persists far downstream. These transition patterns suggested a key to identifying the scale of upstream flow development. By inspection, the lengthscale $\theta = L/R$ used in figure 3 nearly matches stages of kinematically similar axial development over a range of flow rates, for a given inlet profile and curvature ratio. Thus axial flow development must be largely inviscid, and in this section we shall show this quantitatively for the developing axial profile in the central core.

The patterns of developing axial flow can be displayed to advantage using

isovelocity contours, which emphasize the two-dimensional nature of the flow structures. These contours were constructed from our pulsed-probe data by linearly interpolating within the cross-sectional grid of pointwise velocity components. The downstream evolution of a flat inlet profile is compared in figures 4(*a–d*) for all experimental cases, and reveals three characteristic stages of development. Initially, at 20° of bend, flow is shifted strongly towards the inside of the pipe by the potential line vortex. An intermediate stage is characterized by the formation of a 'crescent' of high-velocity fluid moving progressively towards the outside of the bend. The presence of local velocity maxima that are offset from the central axis suggests a convective effect of transverse currents, which sweep outwards centrally and inwards peripherally. Moreover, as axial flow shifts outwards the boundary layer becomes highly non-uniform: progressively thickening on the inner wall, while thinning significantly along the outside. By 180° of bend, this stage has been superseded by contours aligned more nearly parallel to the vertical axis of the pipe, as centrifugal force becomes dominant. Peak velocities are confined to a single region, centred on the symmetry plane near the outside of the pipe bend.

Thus it is apparent, in figures 3 and 4, that axial flow patterns undergo significant transverse shifts as development proceeds stagewise. This flow shift can be quantified by computing the first moment, or centre of momentum, of each axial profile:

$$\left\langle \frac{X}{a} \right\rangle = \frac{\int_{-\frac{1}{2}\pi}^{\frac{1}{2}\pi} \int_{0}^{a} (WX/a)\, r \,\mathrm{d}r \,\mathrm{d}\phi}{\int_{-\frac{1}{2}\pi}^{\frac{1}{2}\pi} \int_{0}^{a} W r \,\mathrm{d}r \,\mathrm{d}\phi}. \tag{2}$$

Integration of (2) was carried out numerically over the Cartesian grid of velocity components defined by the probe traverses, analogous to the computation of flow rate. Resulting stagewise values of $\langle X/a \rangle$ are found to develop on an axial scale a for *both* flat (figure 5*a*) and parabolic (figure 5*b*) inlet profiles. In figure 5(*a*) there appears to be no effect of Reynolds number over entrance lengths $L \leqslant 6a$. Instead, each experimental case first shifts inwards, crosses the pipe axis at $L \approx 2.4a$, and tends monotonically towards an ultimate flow pattern that is split approximately 60–40 % between outer and inner halves of the pipe. Only in this last regime do viscous effects become evident.

These results appear to imply that the transverse flow shift develops independently of pipe curvature. Given the underlying importance of the potential vortex, whose intensity does depend on R/a, this outcome was unexpected. Nevertheless this conclusion is corroborated by computations derived from data of Agrawal *et al.*, which are included in figure 5(*a*).

By comparing figures 5(*a*) and 5(*b*), the effect of the inlet condition can be seen to extend far beyond $L = 6a$, into a downstream region where Re is important. The parabolic inlet cases produce values of $\langle X/a \rangle$ at $L = 25.1a$ that diverge markedly from the sequences followed by flat-inlet cases, as indicated by the dashed lines. These differences are far greater than can be accounted for by any flow asymmetry between upper (U) and lower (L) halves of the pipes, and thus support the view of Yao & Berger that the asymptotic stage of flow development is quite extended.

To complete the description of developing flow, downstream sequences of secondary currents evolving from flat inlet profiles are presented in figures 6(*a–d*), for each Re and curvature ratio. In all cases boundary-layer current is already strong 20° into the bend, in accord with Agrawal's observations. This current initially is most intense

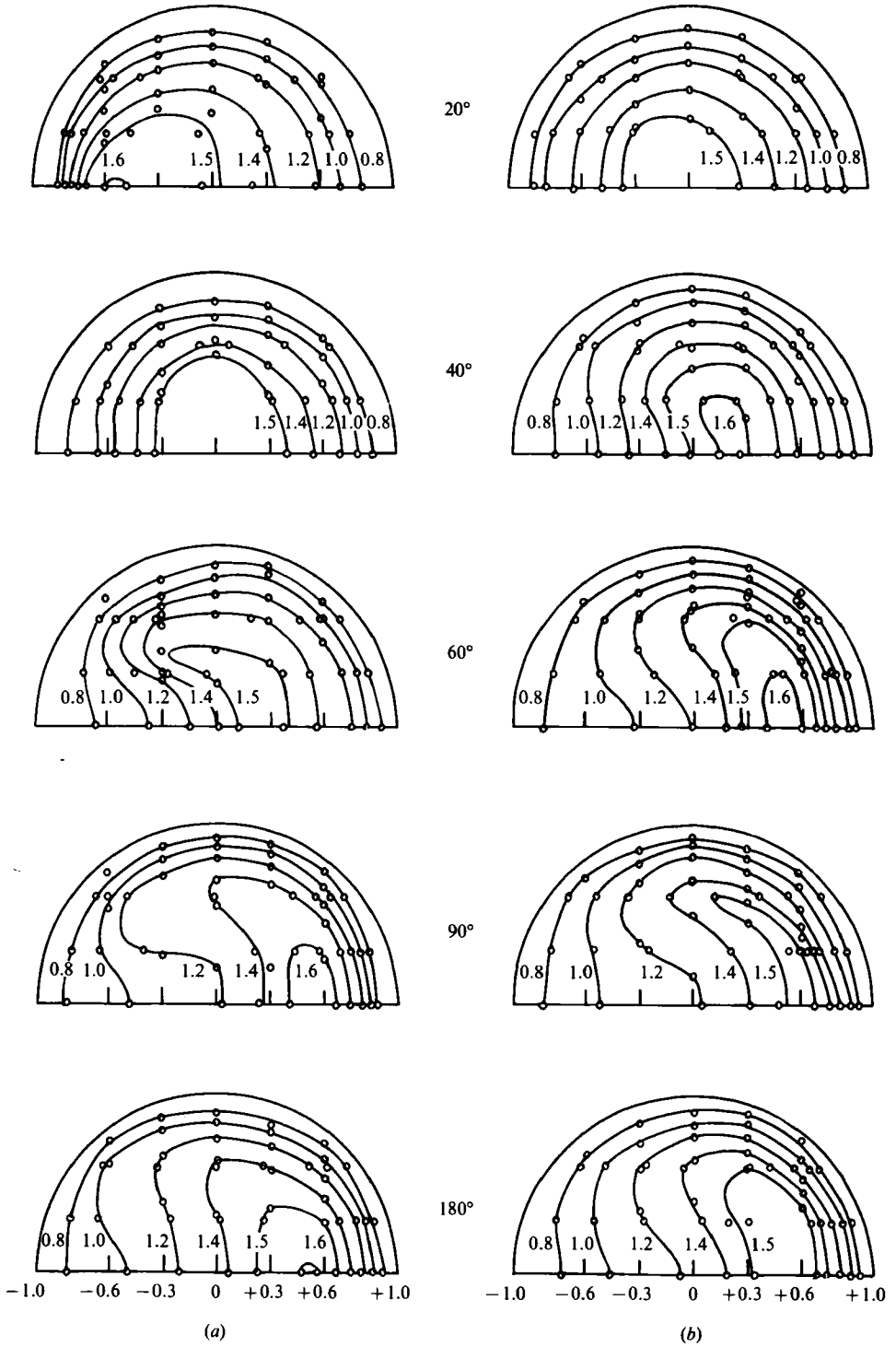

FIGURE 4 (*a*, *b*). For description see opposite.

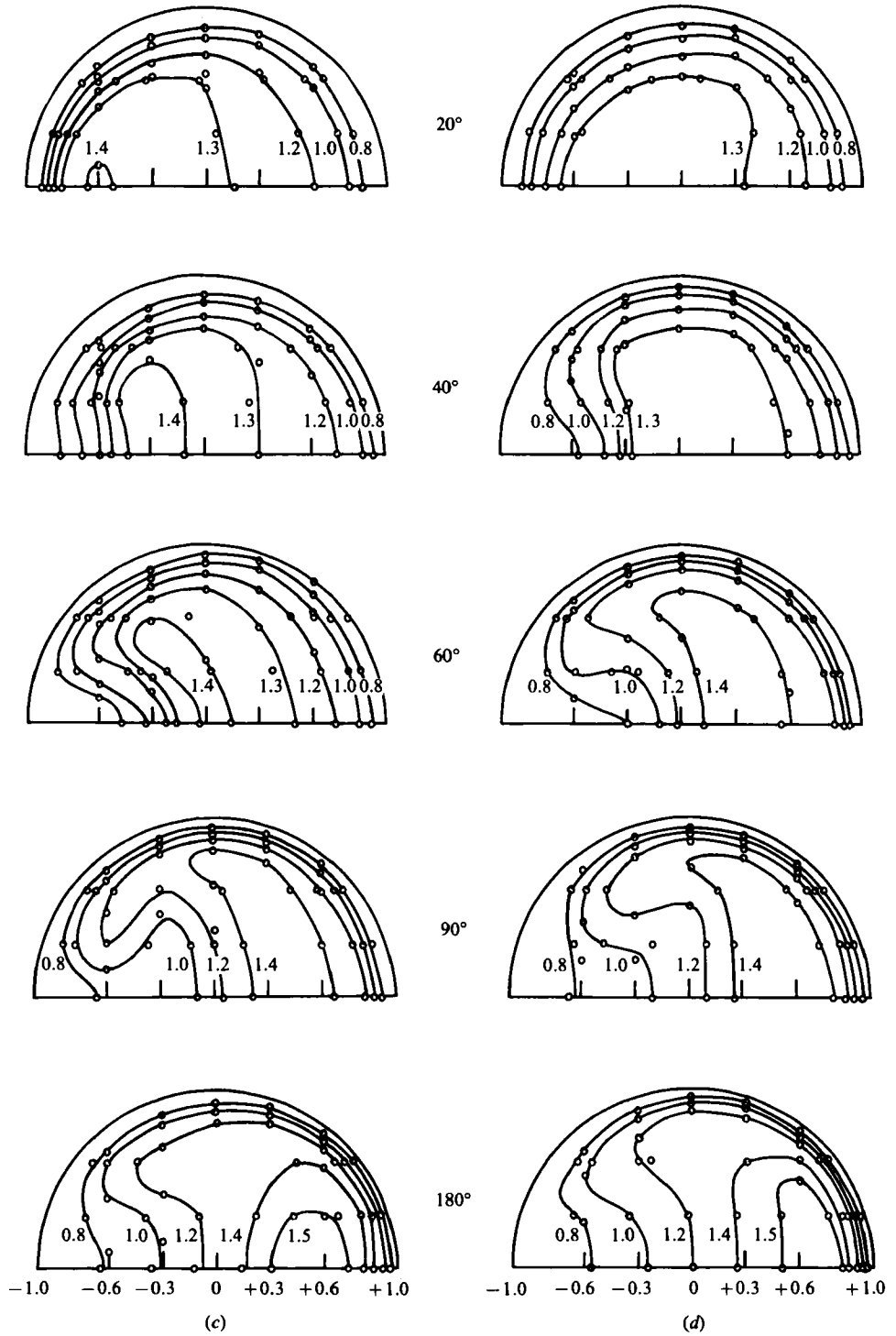

FIGURE 4. Axial isovelocity contours within the first 180° of curved pipes, flat inlet profile. Horizontal axis is non-dimensional pipe radius, with −1.0 at inner wall of bend. (*a*) $R/a = 4.66$, $\kappa = 140$, $\overline{W} = 12.1$ cm/s; (*b*) 8.0, 103, 11.8 cm/s; (*c*) 4.66, 500, 43.8 cm/s; (*d*) 8.0, 390, 44.6 cm/s. Each contour is normalized to the mean axial velocity $\overline{W}$.

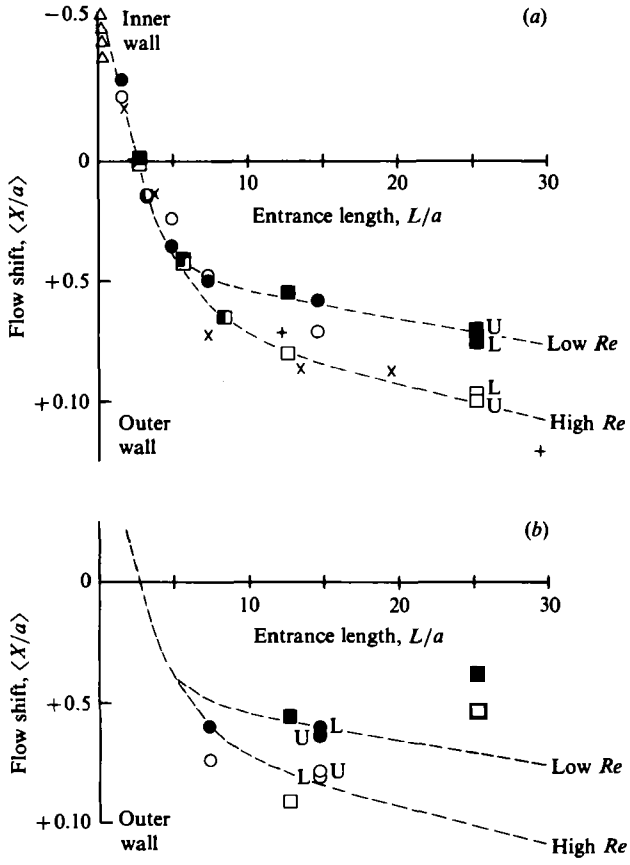

FIGURE 5. The downstream evolution of transverse shifts in axial velocity, expressed as the first moment $\langle X/a \rangle$ versus entrance length in units of pipe radius a, for (*a*) flat and (*b*) parabolic inlet profiles. Closed symbols, $Re = 300$; open symbols, $Re = 1100$; circles, $R/a = 4.66$; squares, $R/a = 8.0$; triangles, inlet data from hot-wire anemometry. U ≡ upper half of pipe cross-section; L ≡ lower half. ×, +, derived from data of Agrawal *et al.* (1978) for water–glycerol solutions: $R/a = 7$, $\kappa = 183$ and $R/a = 20$, $\kappa = 565$ respectively. The dashed lines trace the sequence of developing flat profiles, and thus in (*b*) indicate that flow did not become developed.

along the vertical axis lying perpendicular to the symmetry plane, but at 40° begins to favour the inner wall (compare P with P′ in figure 6*d*). As shown below, this shift coincides with a pronounced increase in axial vorticity. Downstream, the maximal current reverts to the vertical axis, while decreasing as much as threefold. Hence this 'overshoot' in secondary current is characterized by changes in both distribution and magnitude throughout the region of flow development, analogous to the transverse swings in the axial velocity profile.

Swirl intensity is sometimes estimated experimentally by means of a helical pitch $\mathscr{P}$, defined as the axial length required for a fluid parcel entrained in an eddy to trace a complete circuit:

$$\mathscr{P} \equiv \oint \frac{\text{local axial velocity}}{\text{local eddy velocity}} \, \mathrm{d}s.$$

However, eddy patterns associated with these developing currents are not kinematically similar to the closed eddies of developed flow. As seen in figure 6, the central

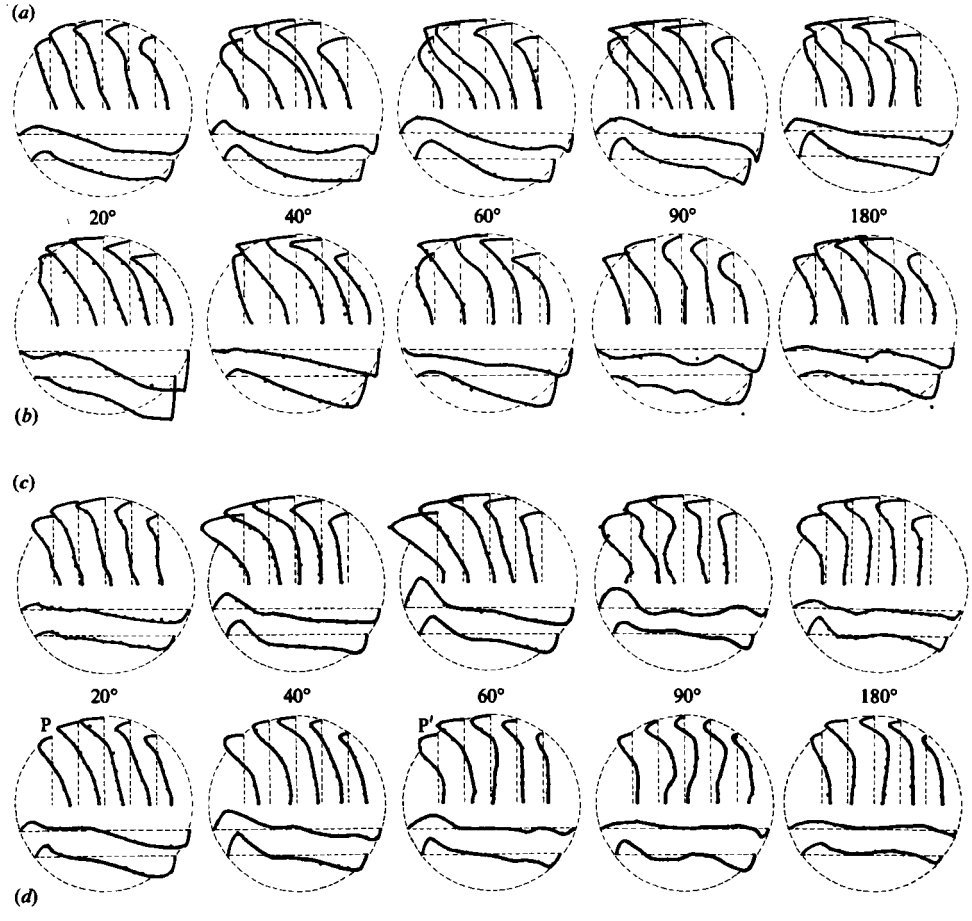

FIGURE 6. X and Y secondary velocity profiles within the first 180° of curved pipes, flat inlet profile. Locations of traverses as in figure 1. Horizontal traces are transposed from upper half of pipe, and thus are shown inverted. (*a*) $R/a = 4.66$, $\kappa = 140$, $\overline{W} = 12.1$ cm/s; (*b*) 8.0, 103, 11.8 cm/s; (*c*) 4.66, 500, 43.8 cm/s; (*d*) 8.0, 390, 44.6 cm/s. Note the shift in the position of peak boundary-layer current from P to P′. All secondary velocities are normalized to $\overline{W}$.

cross-flows exhibit highly non-uniform motions; in some instances they may even reverse their usual outward movement, as inferred by Hawthorne (1951) from measurements of total pressure. The circulating eddies of the more developed flow pattern seen in figure 8 have a pitch of about 25 diameters, which is consistent with Taylor's (1929) observations of dye traces entrained in the boundary-layer of fully developed flow. Clearly, pitch yields a much weaker estimate of eddy strength than the patterns in figure 6 would suggest. This is because cross-flows in the inviscid core are much smaller than the local axial velocities. Thus pitch is limited by the weak central cross-flows, and is insensitive to the strong boundary-layer currents.

Rather than pitch, these secondary currents are better quantified by defining circulation loops typical of the inviscid core (figure 7*a*), the 'maximal' circulation (figure 7*b*) and the boundary layer (figure 7*c*). The maximal and boundary-layer paths were chosen so as to maximize circulation, while the inviscid loop was a fixed path

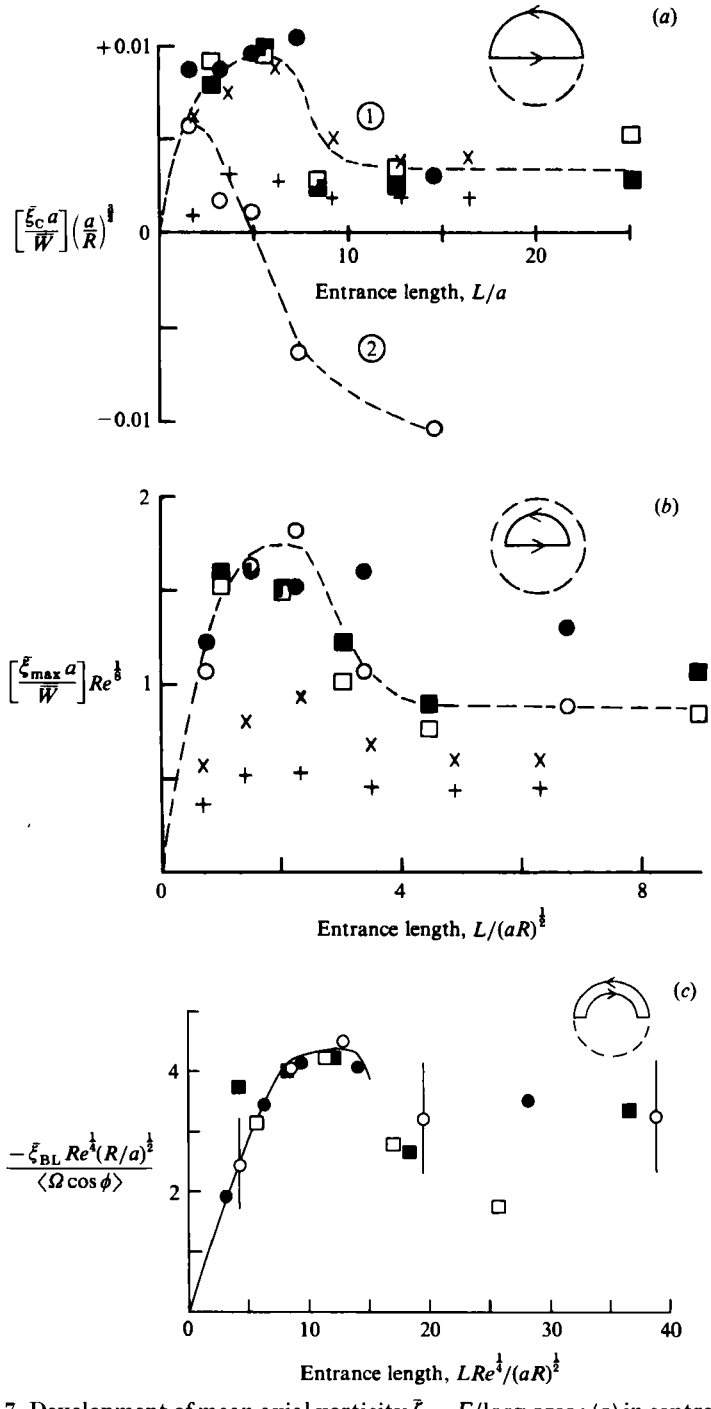

FIGURE 7. Development of mean axial vorticity $\bar{\xi} = \Gamma/\text{loop area}$: (*a*) in central core, on a lengthscale a; (*b*) on maximal circulation path, on a lengthscale $(aR)^{\frac{1}{2}}$; (*c*) in boundary layer, on a lengthscale $(aR)^{\frac{1}{2}}/Re^{\frac{1}{4}}$. Solid line in (*c*) is derived from Hawthorne's inviscid theory (6). Closed symbols, $Re = 300$; open symbols, $Re = 1100$; circles, $R/a = 4.66$; squares, $R/a = 8.0$ ×, +, derived from data of Agrawal *et al.* (1978) for water–glycerol solutions: $R/a = 7$, $\kappa = 138$ and 678 respectively.

enclosing half the pipe cross-section, and thus reflects the total circulation. The circulation integrals were evaluated using the approximation

$$\Gamma = \bar{\xi}\mathscr{A}_{\text{loop}} = \oint \boldsymbol{v}\cdot \mathrm{d}s \approx \sum_i [U_i\,\Delta x_i + V_i\,\Delta y_i],$$

where U_i and V_i are the mean X- and Y-velocities on the ith path segment $(\Delta x_i, \Delta y_i)$.

All the circulation loops show a pattern of rapid initial growth in streamwise vorticity $\bar{\xi}$, followed by a pronounced overshoot in $\bar{\xi}$ within two diameters downstream of the inlet. The occurrence of vorticity overshoot in both the boundary layer ($\bar{\xi}_{\text{BL}}$) and central core ($\bar{\xi}_{\text{C}}$) suggests that these secondary motions are coupled, although in detail their development is somewhat different. As described below, transverse motion in the central core evolves on a lengthscale a, while boundary-layer swirl develops on an upstream scale $(aR)^{\frac{1}{2}}$.

The initial strength of secondary currents in the central core must be a consequence of how the potential line vortex forms and intensifies. Thus it is plausible that these currents should develop on the same lengthscale a as do the axial velocities. When $\bar{\xi}_{\text{C}}$ is scaled non-dimensionally to account for both Agrawal's results and ours, two distinct modes of flow development seem to occur, as indicated by the numbered dashed lines in figure 7(*a*). At low Dean numbers κ (path 1), $\bar{\xi}_{\text{C}}$ intensifies early in the bend and then subsides much as do the other circulation integrals. At higher κ (path 2) the degree of early intensification is not as prevalent, reflecting the reversal of central secondary currents seen in figure 6(*c*). Agrawal's high-κ case is noteworthy in that it appears to trace a transition path from one mode to the other. Yao & Berger have in fact suggested that such motions of the central core could be quite different for low and high κ, owing to the relatively greater importance of centrifugal effects in the latter case.

Both maximal-circulation loops (figure 7*b*) and boundary-layer paths (figure 7*c*) are better correlated with the lengthscale $(aR)^{\frac{1}{2}}$. Each data set shows only a small dependence on Re; and the initial growth of boundary-layer swirl is actually inviscid, as will be shown in the discussion to follow. Maximal loops applied to Agrawal's data yield estimates of $\bar{\xi}_{\text{max}}$ that show qualitatively this same growth and relaxation.† This common pattern observed over a range of Dean numbers implies that the initial development of boundary-layer currents is kinematically similar in all cases if entrance lengths are scaled to Yao's upstream scale $(aR)^{\frac{1}{2}}$.

We have already remarked that our flow sections must have been too short to allow the completion of axial flow development. It is also doubtful whether secondary currents became fully developed even after 180° of bend angle, as can be inferred by comparing an example of downstream secondary currents resulting from parabolic inlet flow, in figure 8, with the corresponding cases for flat inlet profiles in figure 6. The central cross-flows at 180° of bend are noticeably different, and the parabolic case displays twin secondary vortices imbedded in the large-scale vortex pair. Thus entrance lengths in curved pipes extend through $12\,(aR)^{\frac{1}{2}}$, for the moderate values of κ used in this study. Verifying the downstream scale $(aR\kappa)^{\frac{1}{2}}$ proposed by Yao & Berger would require a much wider range of curvature ratios, as well as smaller margins of experimental uncertainty!

Varieties of the four-vortex structure seen in figure 8 have been reported previously by several authors. Agrawal *et al.* interpreted transverse flow reversals, arising near the inner wall at $L/a = 6.11$ $(2.3\,(aR)^{\frac{1}{2}})$ for $\kappa = 678$, as secondary vortex pairs

† As Agrawal's published data include only one transverse velocity component, a quantitative comparison with our results is not possible except in the case of figure 7(*a*).

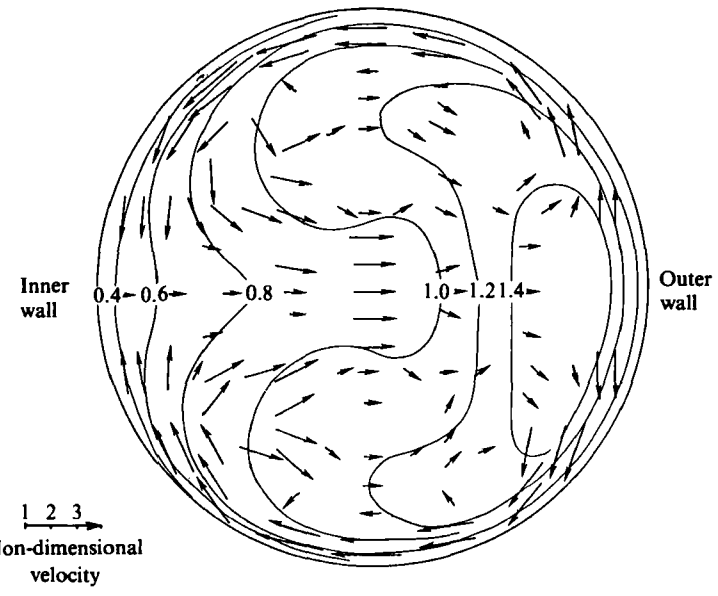

FIGURE 8. Axial isovelocity contours at 180° of bend for parabolic inlet profile, $R/a = 4.66$, $\kappa = 510$, $\overline{W} = 45$ cm/s. Superimposed arrows show the direction of transverse velocities, with relative magnitudes scaled by the arrow lengths. From Olson *et al.* (1984); reproduced by permission of ASME.

imbedded within the Dean-type swirl. They reported that vestiges of this structure could be traced through $L/a = 16.49\ (6.2\,(aR)^{\frac{1}{2}})$. Using axisymmetric turbulent inlet flow, Rowe (1970) also observed such twin imbedded vortices near the outer pipe wall at 180° of bend, and attributed their origin to the drift of streamwise secondary vorticity. By his proposed mechanism, the secondary currents were weaker at the inner wall, allowing the vortex filaments to drift closer together and form a twin vortex roll-up. This concentrated vorticity would then be propelled toward the outer wall by central cross-flows. Akiyama *et al.* (1983) also have reported that twin imbedded vortices are formed downstream along the outer wall, for laminar parabolic inlet flow.

Of course, our flow sections were too short to resolve whether these features represent a transitional regime, or persist in fully developed flow. The latter outcome would substantiate a recent theoretical result of Dennis & Ng (1982) that solutions to fully-developed curved pipe flow are not unique, and thus depend in principle on inlet conditions. While these authors exhibit a four-vortex numerical solution, the associated axial flow pattern has globally maximal values offset from the centreline of symmetry, a detail which is not seen in either Agrawal's data or ours.

4. Discussion

These experimental results partly confirm theoretical predictions that secondary flows in curved circular pipes develop initially over the inviscid lengthscale $(aR)^{\frac{1}{2}}$ for moderate Dean numbers. Thus Yao's proposed upstream scale appears to be appropriate; but his theory, based on a general conservation of mass and momentum, leaves unexplored how specific flow features may develop. In this section we attempt to relate specific experimental results to other theoretical models of inviscid secondary

flow. These models provide additional grounds for expecting $(aR)^{\frac{1}{2}}$ to be an inviscid lengthscale in curved pipes.

We consider first a theory of vorticity transport in uniform bends as developed by Squire & Winter (1951) and extended by Hawthorne (1951, 1961). Their analyses predict that the growth of secondary streamwise vorticity along a streamline having curvature R and located at an angle $\frac{1}{2}\pi-\phi$ out of the symmetry plane is given by

$$\xi = -2\theta\,\Omega\cos\phi, \tag{3}$$

where Ω is the inlet azimuthal vorticity and θ $(= L/R)$ is the deflection of the streamline over a path length L. As this model neglects viscous effects and streamline displacement, (3) is pertinent only to the initial growth of secondary currents.

In our experiments inlet vortex rings were confined to the wall, so that (3) can be applied only to the growth of secondary currents within the boundary layer. Moreover, as Squire's analysis assumes inviscid flow and neglects boundary-layer growth, we might expect ξ in (3) to overestimate our experimental values $\bar{\xi}_{\mathrm{BL}}$ $(= \Gamma_{\mathrm{BL}}/\text{loop area})$. This relation was tested by estimating the wall velocity gradients $\partial W/\partial r$ $(= \Omega)$ at the inlet to the curved pipes,† averaging over ϕ, and forming the ratio $\bar{\xi}_{\mathrm{BL}}/\langle\Omega\cos\phi\rangle$. The results are shown in figure 7(*c*), using an axial lengthscale $(aR)^{\frac{1}{2}}Re^{-\frac{1}{4}}$ to reconcile upstream inviscid transport and downstream viscous effects. The initial linear slope in this figure represents a regime of inviscid growth, $\bar{\xi}_{\mathrm{BL}} = -0.57\theta\langle\Omega\cos\phi\rangle$, which describes all four experimental cases through at least 20° of bend. While the numerical results differ from a preliminary account of Olson & Snyder (1983) (who used an erroneous value of R/a), it seems clear that the initial growth of secondary currents in the boundary layer agrees qualitatively with Squire's mechanism. We conclude that overshoot may occur because inviscid growth permits the build-up of intense boundary-layer currents long before the axial-velocity profile can be restructured by convection.

As is evident in figure 7(*c*), boundary-layer currents evolving from flat inlet profiles eventually subside to 'asymptotic' values $\bar{\xi}_{\mathrm{BL}}/\langle\Omega\cos\phi\rangle = -(3.1\pm0.7)\,(R/a)^{-\frac{1}{2}}Re^{-\frac{1}{4}}$. The question arises as to why Squire's mechanism ceases to be effective in maintaining initial growth rates downstream from $L = 2\,(aR)^{\frac{1}{2}}$. Hawthorne extended this analysis by proposing that the build-up of intense secondary currents would be self-limiting, causing streamlines to be deflected away from regions of high vorticity transport as flow progressed downstream. The effect is implied in (3) by the factor $\cos\phi$, which accounts for the component of streamline acceleration that promotes secondary vorticity. In Hawthorne's formulation, $\alpha = \frac{1}{2}\pi-\phi$ is a measure of streamline twist and depends on the cumulative bend deflection θ. By comparing secondary current with axial velocity, he showed that the net twist α over a uniformly curved bend could be approximated by an elliptic function of θ, analogous to the large-scale periodic motion of a pendulum.

From this result Hawthorne predicted that streamlines should turn first towards the inner wall, then outwards, as flow proceeded downstream. For inlet turbulent airflow, he observed that the streamline of maximal total pressure shifted downstream in accord with this theory, reversing its twist at sites very near the theoretical zeroes of his solution. To account for this motion he inferred that the secondary currents themselves must periodically reverse their rotation.

† Inlet wall gradients were evaluated by extrapolating hot-wire data at $0.8r/a$ out to the wall. For our entrance bell this location yielded the most consistent readings, while still being within the vortex ring. An analogous averaging procedure applied to a parabolic profile would yield better than 1 % agreement between extrapolated and actual mean gradients.

	$R/a = 4.66$			$R/a = 8.0$		
$\overline{W} = 12$ cm/s	1.00	(1.41)†	(5.65)‡	1.03	(1.41)†	(5.92)‡
$\overline{W} = 44$ cm/s	0.79	(1.41)†	(4.52)‡	0.74	(1.41)†	(3.95)‡

TABLE 2. Peak values of boundary-layer vorticity $(R/a)^{\frac{1}{2}}\ (-\bar{\xi}_{\mathrm{BL}}/\langle\Omega\cos\phi\rangle)$ compared with models of:

† Hawthorne: $(R/a)^{\frac{1}{2}}\ (-\bar{\xi}_{\mathrm{BL}}/\langle\Omega\cos\phi\rangle) = 1.41$
‡ Squire & Winter: $(R/a)^{\frac{1}{2}}\ (-\bar{\xi}_{\mathrm{BL}}/\langle\Omega\cos\phi\rangle) = 2(R/a)^{\frac{1}{2}}\theta$

To apply Hawthorne's (1951) theory, which was formulated for a linear inlet-velocity profile, we adapt his derivation to the evolution of an inlet wall vortex ring. It is convenient to start with his equation (14), which is a generalized form of our (3). Like Hawthorne, we assume the axial velocity remains unchanged along a streamline, so that

$$\chi \equiv \frac{\xi_{\mathrm{BL}}}{\Omega} = -2\int_0^{\theta} \cos\alpha \,\mathrm{d}\theta' \tag{4a}$$

To solve this equation an additional relation between α and θ must be determined. Using Hawthorne's method, we assume that the incremental twist $\mathrm{d}\alpha$ of a streamline in the boundary layer of thickness δ, in a pipe of radius a, can be related to a deflection $V_\phi\,\mathrm{d}t$ by

$$a\,\mathrm{d}\alpha = V_\phi\,\mathrm{d}t. \tag{4b}$$

In (4b) the mean azimuthal velocity V_ϕ is approximated using Stokes' Theorem

$$V_\phi \pi a = \xi_{\mathrm{BL}} \pi a\,\delta,$$

and the time increment $\mathrm{d}t$ is expressed as $\mathrm{d}t = R\,\mathrm{d}\theta/\frac{1}{2}\overline{W}$, where $\frac{1}{2}\overline{W}$ is taken to be the mean axial velocity in the boundary layer. From these expressions, noting that $\Omega \approx \overline{W}/\delta$, we obtain

$$\mathrm{d}\theta = \frac{\overline{W}}{2}\frac{a}{R}\frac{1}{\xi_{\mathrm{BL}}\delta}\mathrm{d}\alpha \simeq \frac{1}{2\chi}\frac{a}{R}\mathrm{d}\alpha.$$

Substituting this expression for $\mathrm{d}\theta$ into (4a) and differentiating with respect to α, we find

$$\chi\frac{\mathrm{d}\chi}{\mathrm{d}\alpha} = -\frac{a}{R}\cos\alpha,$$

and after integrating

$$\chi^2 = -2\frac{a}{R}\sin\alpha,$$

since $\chi(0) = 0$. This result implies that streamwise vorticity is maximal at $|\alpha| = \frac{1}{2}\pi$. When inlet vorticity Ω is effectively averaged over all streamlines by the weighting factor $\cos\phi$, the following expression is obtained:

$$\left|\frac{\bar{\xi}_{\mathrm{BL}}}{\langle\Omega\cos\phi\rangle}\right|_{\mathrm{peak}} = 1.41\left(\frac{a}{R}\right)^{\frac{1}{2}}. \tag{5}$$

Peak experimental values of $\bar{\xi}_{\mathrm{BL}}$ are compared in table 2 with predictions based on Squire's theory (3) and Hawthorne's extended result (5). The numerical coefficient obtained experimentally, 0.89 ± 0.15, is approximately two-thirds that predicted by (5), and seems to depend somewhat on fluid velocity. The downstream sites of peak

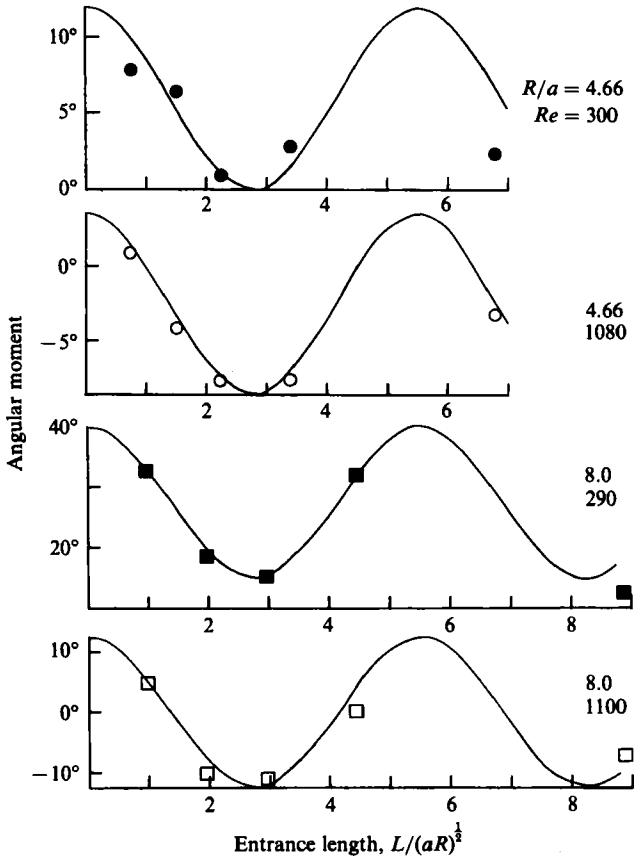

FIGURE 9. The downstream twist of peak boundary-layer current, as quantified by the angular moment

$$\langle\phi\rangle = \int_{-\frac{1}{2}\pi}^{\frac{1}{2}\pi} V_\phi \phi \, \mathrm{d}\phi \Big/ \int_{-\frac{1}{2}\pi}^{\frac{1}{2}\pi} V_\phi \, \mathrm{d}\phi.$$

Each experimental case is fitted to the function

$$\langle\phi\rangle = A + B \sin[\pi L/2.75\,(aR)^{\frac{1}{2}}].$$

The amplitude B is constant for a given curvature ratio R/a.

$\bar{\xi}_{\mathrm{BL}}$ also are velocity-dependent, being distributed between 2–3 $(aR)^{\frac{1}{2}}$ among our four experimental cases. These details are not predicted by either theoretical model, and may be due to viscous effects, accounting for the factor $Re^{-\frac{1}{4}}$ in the axial lengthscale. Frictional effects can be incorporated empirically into this model by approximating α, an elliptic integral, as

$$\alpha \approx \left[\frac{L\,Re^{\frac{1}{4}}}{2.75^2\,(aR)^{\frac{1}{2}}}\right]^2 \left[1 - 0.05\left(\frac{L\,Re^{\frac{1}{4}}}{2.75^2\,(aR)^{\frac{1}{2}}}\right)^4\right]$$

and

$$\chi = 4.3\left(\frac{a}{R}\right)^{\frac{1}{2}} Re^{-\frac{1}{4}} \sin^{\frac{1}{2}}\alpha. \tag{6}$$

Expression (6) is represented by the solid line in figure 7(*c*). An effect of friction is seen to reduce the initial growth of swirl by a factor of three, compared with Hawthorne's inviscid model.

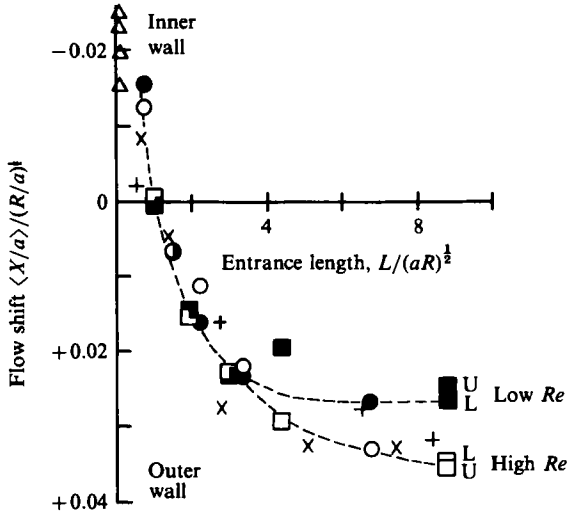

FIGURE 10. A hypothetical scaling of the transverse flow shift $\langle X/a \rangle$ to the lengthscale $(aR)^{\frac{1}{2}}$. Symbols as in figure 5. This formulation predicts $\langle X/a \rangle \geqslant 1$ for $R/a \geqslant 900$, and therefore can be valid only for a limited range of tightly coiled pipes.

Thus streamline twist appears to account qualitatively for the dampening of downstream secondary currents. Hawthorne's model also reconciles the lengthscale $(aR)^{\frac{1}{2}}$, derived by Yao from considerations of mass and momentum conservation, with the scale R over which Squire's mechanism promotes secondary vorticity. If twist extends far downstream, it also supports Rowe's account of how imbedded vortices could first form at $15\,(aR)^{\frac{1}{2}}$.

Hawthorne was well aware of certain shortcomings in his model, observing that friction was a major factor tending to reduce, rather than promote, secondary circulation in bends. Nonetheless the agreement between theory and experiment is intriguing primarily because the basic premise regarding azimuthal motion is incorrect: neither our data nor those of Agrawal ever show the reversal of boundary-layer current that is assumed to invert the twist! Notwithstanding, we have observed that peak boundary-layer currents do undergo periodic azimuthal shifts. By taking the first angular moment of peak boundary-layer current,

$$\langle \phi \rangle = \frac{\int_{-\frac{1}{2}\pi}^{\frac{1}{2}\pi} [V_\phi]_{\text{peak}}\, \phi \, \mathrm{d}\phi}{\int_{-\frac{1}{2}\pi}^{\frac{1}{2}\pi} [V_\phi]_{\text{peak}}\, \mathrm{d}\phi},$$

with $V_\phi = V_y \sin\phi - V_x \cos\phi$, we have quantified this twist effect for each of the flow patterns shown in figures 6(*a–d*). As summarized in figure 9, in every case the sense of twist evolves consistently on a lengthscale $(aR)^{\frac{1}{2}}$ and extends far downstream. Perhaps this effect is related to certain 'elastic' phenomena, known to be induced in rotating fluids by the presence of vorticity.

It remains unclear why the axial flow shift should scale with a, implying that pipe curvature has no influence on how axial profiles or transverse currents develop in curved pipes. This result conflicts with physical intuition, so that we consider an alternative formulation in figure 10. By normalizing the flow shift $\langle X/a \rangle$ to $(R/a)^{\frac{1}{2}}$,

the data in figure 5(*a*) can be rescaled to the lengthscale $(aR)^{\frac{1}{2}}$. Admittedly we know of no rationale for this normalization procedure, which in any case cannot be valid for loosely coiled pipes: figure 10 predicts the physically impossible result $\langle X/a \rangle > 1$ for $R/a > 900$. Nonetheless this formulation correlates all the experimental data equally as well as figure 5, and supports the use of the scale $(aR)^{\frac{1}{2}}$ for both axial profiles and boundary-layer swirl.

Both the axial flow shift and the transverse currents depend on the interaction of the inviscid core vortex with centrifugal force. Thus further study of the developing potential vortex is needed to understand why axial profiles develop as they do. In Singh's theoretical formulation of entry flow the potential vortex emerges abruptly from a uniform injection velocity and is only subsequently modified by boundary-layer development. Likewise, Agrawal's data demonstrate that this flow structure is already nearly developed at $0.7\,(aR)^{\frac{1}{2}}$, so that the entire region of interest lies very near the inlet, where further experimental study is likely to be difficult. We think that theorists might be better placed to resolve how these flow structures arise, and whether their development can be described by a single upstream lengthscale.

5. Conclusions

Developing axial profiles and secondary currents in tightly-curved pipes evolve on separate lengthscales, a and $(aR)^{\frac{1}{2}}$ respectively, over a range of moderate inlet Dean numbers. This experimental study confirms that the upstream development of these flow structures is largely inviscid and is compatible with theoretical models of secondary flow development by Squire & Winter, Hawthorne and Singh.

Both our study and that of Agrawal *et al.* used fluids of similar kinematic viscosity (~ 0.1 cSt) in pipes of the same diameter (3.8 cm inner diameter), so that the scaling rules we propose can be substantiated only in part. It would be useful to complement these investigations using other fluids of different kinematic viscosities, over a wide range of curvature ratios.

REFERENCES

Agrawal, Y., Talbot, L. & Gong, K. 1978 Laser anemometry study of flow development in curved circular pipes. *J. Fluid Mech.* **85**, 497–518.

Akiyama, M., Hanaoka, Y., Cheng, K. C., Urai, I. & Suzuki, M. 1983 Visual measurements of laminar flow in the entry region of a curved pipe. In *Proc. 3rd Intl Symp. on Flow Visualization, Ann Arbor* (Ed. Wen-Jei Yang), pp. 756–760.

Dennis, S. C. R. & Ng, M. 1982 Dual solution of steady laminar flow through a curved tube. *Q. J. Mech. Appl. Maths* **35**, 305–324.

Hawthorne, W. R. 1951 Secondary circulation in fluid flow. *Proc. R. Soc. Lond.* A **206**, 374–387.

Hawthorne, W. R. 1961 Flow in bent pipes. In *Proc. Sem. on Aeronautical Science, National Aeronautical Laboratory, Bangalore, India*, pp. 307–333.

Humphrey, J. A. C., Taylor, A. M. K. & Whitelaw, J. H. 1977 Laminar flow in a square duct of strong curvature. *J. Fluid Mech.* **83**, 509–527.

Olson, D. E. 1971 Fluid mechanics relevant to respiration: flow within curved or elliptical tubes and bifurcating systems. Ph.D. thesis, University of London.

Olson, D. E., Parker, K. H. & Snyder, B. 1984 A pulsed wire probe for the measurement of velocity and flow direction in slowly moving air. *Trans. ASME* K: *J. Biomech. Engng* **106**, 72–78.

Olson, D. E. & Snyder, B. 1983 The growth of swirl in curved circular pipes (Letter). *Phys. Fluids* **26**, 347–349.

ROWE, M. 1970 Measurements and computations of flow in pipe bends. *J. Fluid Mech.* **43**, 771–783.

SINGH, M. P. 1974 Entry flow in a curved pipe. *J. Fluid Mech.* **65**, 517–539.

SQUIRE, H. B. & WINTER, K. G. 1951 The secondary flow in a cascade of airfoils in a non-uniform stream. *J. Aero. Sci.* **18**, 271–277.

TAYLOR, G. I. 1929 The criterion for turbulence in curved pipes. *Proc. R. Soc. Lond.* A **124**, 243–249.

YAO, L.-S. & BERGER, S. A. 1975 Entry flow in a curved pipe. *J. Fluid Mech.* **67**, 177–196.